

In-Line Phase Contrast Imaging of Hepatic Portal Vein Embolization with Radiolucent Embolic Agents in Mice: A Preliminary Study

Rongbiao Tang^{1*}, Wei Huang¹, Fuhua Yan¹, Yong Lu¹, Wei-Min Chai¹, Guo-Yuan Yang², Ke-Min Chen^{1*}

1 Department of Radiology, Rui Jin Hospital, Shanghai Jiao Tong University School of Medicine, Shanghai, People's Republic of China, **2** Neuroscience and Neuroengineering Center, Med-X Research Institute, Shanghai Jiao Tong University, Shanghai, People's Republic of China

Abstract

It is crucial to understand the distribution of embolic agents inside target liver during and after the hepatic portal vein embolization (PVE) procedure. For a long time, the problem has not been well solved due to the radiolucency of embolic agents and the resolution limitation of conventional radiography. In this study, we first reported use of fluorescent carboxyl microspheres (FCM) as radiolucent embolic agents for embolizing hepatic portal veins. The fluorescent characteristic of FCM could help to determine their approximate location easily. Additionally, the microspheres were found to be fairly good embolizing agents for PVE. After the livers were excised and fixed, they were imaged by in-line phase contrast imaging (PCI), which greatly improved the detection of the radiolucent embolic agents as compared to absorption contrast imaging (ACI). The preliminary study has for the first time shown that PCI has great potential in the pre-clinical investigation of PVE with radiolucent embolic agents.

Citation: Tang R, Huang W, Yan F, Lu Y, Chai W-M, et al. (2013) In-Line Phase Contrast Imaging of Hepatic Portal Vein Embolization with Radiolucent Embolic Agents in Mice: A Preliminary Study. PLoS ONE 8(12): e80919. doi:10.1371/journal.pone.0080919

Editor: Jonathan A. Coles, Glasgow University, United Kingdom

Received: August 14, 2013; **Accepted:** October 18, 2013; **Published:** December 4, 2013

Copyright: © 2013 Tang et al. This is an open-access article distributed under the terms of the Creative Commons Attribution License, which permits unrestricted use, distribution, and reproduction in any medium, provided the original author and source are credited.

Funding: This research was supported by the Natural Science Foundation of China (Grant no. 81301347 and 81271740) and Nation Basic Research Program of China (973 Program 2010CB834305). The funders had no role in study design, data collection and analysis, decision to publish, or preparation of the manuscript.

Competing Interests: The authors have declared that no competing interests exist.

* E-mail: tangme8688258@sina.com (RT); keminchenrj@163.com (KMC)

Introduction

Preoperative portal vein embolization (PVE) is an effective modality to induce hepatic hypertrophy by obstructing the selective portal vein supplying the diseased segment of the liver [1–4]. In order to prevent blockage in the wrong region, it is quite essential to determine the distribution of the embolic agents inside target liver during and after the embolization. Clinically, gelatin sponge (GS) and polyvinyl alcohol particles (PVA) are the most commonly used embolic agents [5,6]. However, GS and PVA are low-absorption materials which are hardly visualized by conventional radiography. Therefore, embolic agents are always injected by combining them with iodine contrast agent to enhance image contrast. Nevertheless, iodine-enhanced method only indirectly shows the embolization site, and can not accurately verify the distribution of embolic agents. Additionally, it is still difficult to show fine embolized vessels with a diameter of 200 μm or less by conventional angiography due to the limitation of spatial resolution [7].

To overcome the challenges, novel imaging method should be applied. Currently, synchrotron radiation (SR) phase contrast imaging (PCI) has been widely utilized to provide excellent image contrast for soft tissues [8–11]. PCI, utilizing the phase shift, can produce higher contrast images than absorption contrast imaging (ACI) [12,13]. Also, PCI is considered as a powerful preclinical imaging modality to observe fine structures with its resolution higher than any available clinical radiography [14,15]. Using PCI, hepatic vessels down to micron level can be clearly shown without

using contrast agents [16,17]. The values of these applications raise the possibility of using PCI for clearly imaging low-absorption embolic materials.

In this study, GS and PVA were imaged by SR imaging. PCI and ACI were performed and compared. We evaluated the feasibility of using PCI for imaging PVE with radiolucent fluorescent carboxyl microspheres (FCM).

Materials and Methods

Sample Preparation

All experiments were conducted in accordance with the guidelines established and approved by Shanghai Jiao Tong University's Institutional Animal Care and Use Committee. 6 male ICR mice were anesthetized using an intraperitoneal injection of ketamine (100 mg kg^{-1}) and xylazine (10 mg kg^{-1}). The main portal trunk was dissected, and then punctured with a thin PE-50 catheter through a midline laparotomy. Then PVE was performed by injecting 100 FCM (in 0.1 ml PBS) into the portal vein via the catheter attached to a 1 ml syringe. 5 minutes after the PVE, mice were sacrificed by cervical dislocation under anesthesia. The livers were harvested and placed in 4% formaldehyde solution. The numbers of FCM in main lobes of liver were counted under fluorescence microscope. Data were expressed in mean \pm standard deviation. Three non-dehydrated livers were randomly chosen to scan by phase contrast CT imaging. For imaging dehydrated livers, the other three livers were placed in a 4%

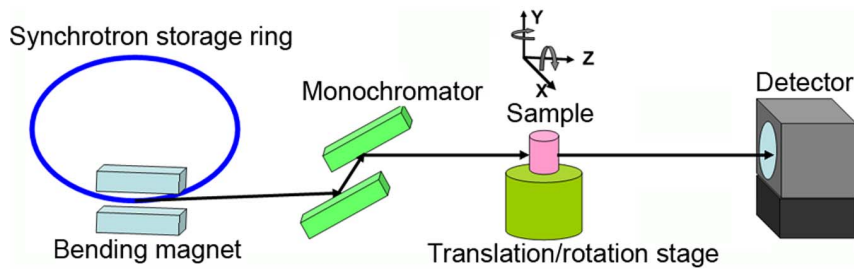


Figure 1. Schematic of the experimental setup for in-line phase contrast imaging at BL13W in SSRF. The sample-to-detector distance has a changeable range of 8 m.
doi:10.1371/journal.pone.0080919.g001

formaldehyde solution for 72 hours, dehydrated with 100% ethanol for 48 hours, and then placed in the air for 2 hours.

SR Imaging Parameters

Imaging was performed at the BL13W1 beamline in Shanghai Synchrotron Radiation Facility (SSRF, China). X-rays were derived from a 3.5 GeV electron storage ring. The beamline covered an energy range of 8 to 72.5 keV. X-Ray was monochromatized at 19 keV energy using a double-crystal monochromator with Si(111) and Si(311) crystals. The energy resolution was $\Delta E/E < 5 \times 10^{-3}$. The transmitted x-rays were first converted to visible light by a scintillator consisting of a 100 μm thick CdWO_4 cleaved single crystal, and then captured by a CCD camera with the pixel size of 3.7 μm . (Photonic Science, UK). Samples were positioned on a translation/rotation stage at a distance of 34 m from the synchrotron source. The distance between the sample and the detector had a changeable range of 8 m (Fig. 1).

Comparison between ACI and PCI

Clinically utilized 150–350- μm GS (Eric Kang, China) and 90–180- μm PVA (PVA-100, Cook) were purchased for imaging. FCM (ACME microspheres, USA) were used for hepatic PVE. FCM had a mean diameter of 100 μm , ranging from 90 to 105 μm . ACI and PCI were performed with the same imaging parameters except sample-to-detector distance ($d = 1 \text{ cm}$ and 60 cm , respectively). The distance was changed by moving the CCD camera on a rail. Relative densities were evaluated by line profile analysis via Image-Pro Plus 6.0.

Phase Contrast CT Imaging

1000 projection images were obtained from each sample over 180° in rotation steps of 0.18° . The projections were recorded with sample-to-detector distance of 60 cm and exposure time of 1 s. The raw data were processed by applying the filtered back projection (FBP) algorithm with PITRE software [18]. 3D phase contrast reconstructed images were acquired by using the Amira 5.2 software (Mercury Computer Systems, USA).

Results

SR Imaging of GS and PVA

The radiolucent characteristic of GS and PVA was demonstrated in Fig. 2. No distinct contrast between GS or PVA and its surrounding air could be observed on the absorption images (Figs. 2c and g). After adjusting the distance to 60 cm, we were able to clearly visualize the GS and PVA on the phase contrast images (Figs. 2d and h). The two embolic agents were both irregular in shape (Figs. 2b and f).

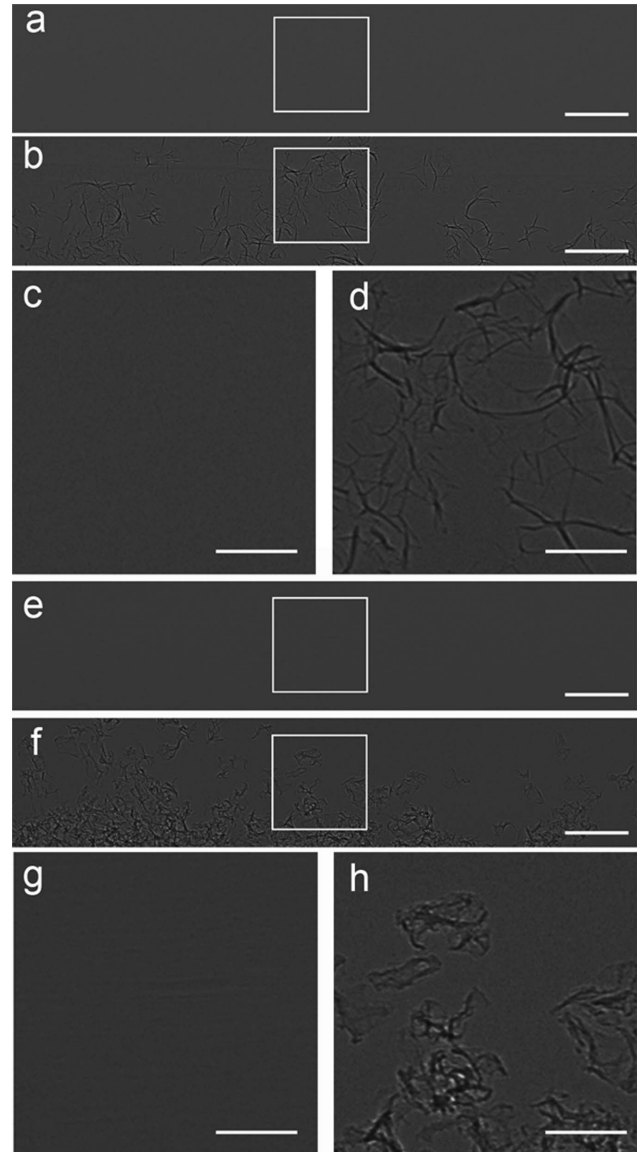


Figure 2. SR images of GS (a-d) and PVA (e-h) at 19 keV with two sample-to-detector distances of 1 cm (a,e) and 60 cm (b,f). (c), (d), (g) and (h) are magnified images of the region in a white box in (a), (b), (e) and (f), respectively. The GS and PVA can be clearly displayed on phase contrast images (b,d,f,h), but not on absorption contrast images (a,c,e,g). GS and PVA were exposed to the air. The pixel size was $3.7 \mu\text{m} \times 3.7 \mu\text{m}$. The exposure time was 1 s. Scale bars, 500 μm (a,b,e,f) and 200 μm (c,d,g,h).
doi:10.1371/journal.pone.0080919.g002

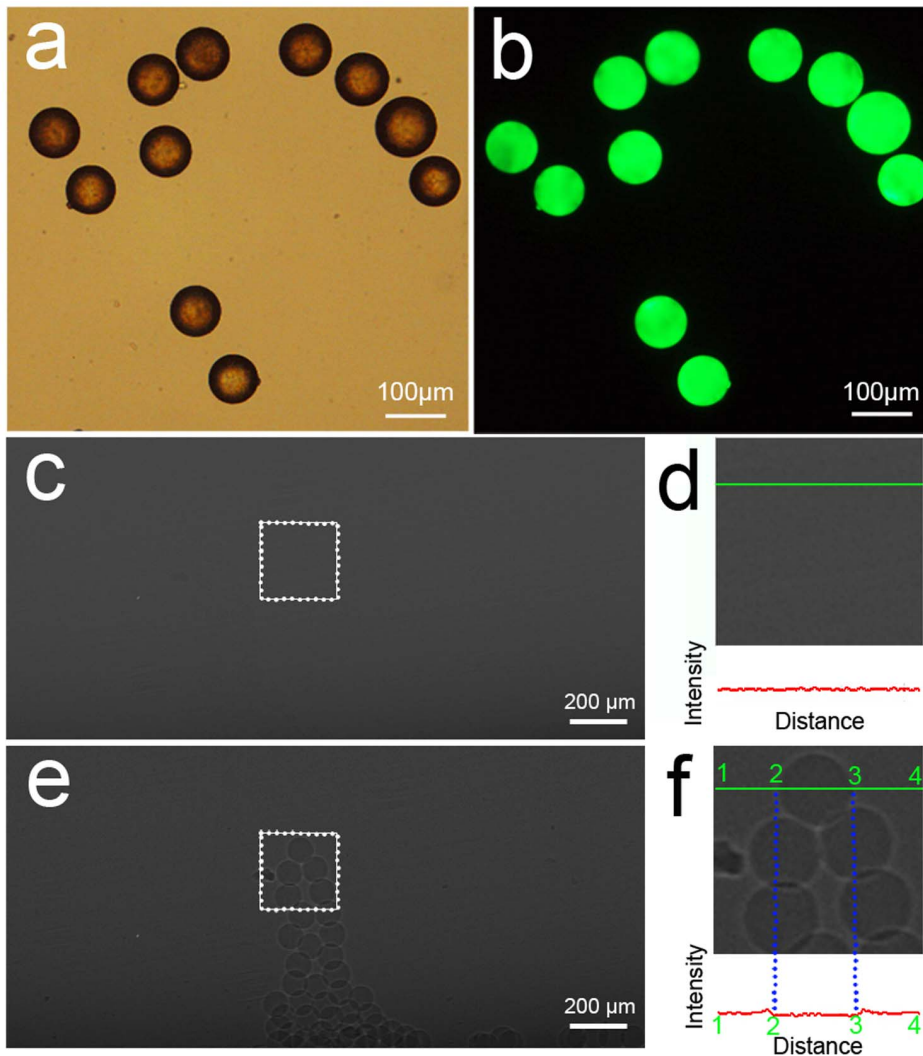


Figure 3. Microscopic observation and SR images of FCM. (a) Optical micrograph shows that FCM are spherical particles with smooth surface. (b) FCM presents bright green fluorescence. (d) and (f) are magnified images of the region in a box in (c) and (e), respectively. The microspheres can be clearly seen on phase contrast image (f), but not on absorption contrast image (d). The intensity values along a straight line (green) were displayed by using line profile analysis (red). Note that the beads caused a reduced change in intensity between the left (2) and right (3) boundaries on the phase contrast image (f). Images were obtained at the energy of 19 keV with two sample-to-detector distances of 1 cm (c) and 60 cm (e). The pixel size was $3.7 \mu\text{m} \times 3.7 \mu\text{m}$; the exposure time was 1 s. doi:10.1371/journal.pone.0080919.g003

Morphological Observation and SR Imaging of FCM

FCM have smooth and uniform surface morphology, as confirmed by optical microscopy (Fig. 3a). The microspheres also present bright green fluorescence (Fig. 3b). In Figs. 3c and d, the images obtained by absorption contrast could not reveal the microspheres at all. In comparison, PCI could provide clear visualization of the microspheres (Figs. 3e and f). The beads caused a visible change in intensity around the edges on the phase contrast image (Fig. 3f). The fluorescent micrograph (Fig. 4b) shows FCM in the liver more clearly than optical micrograph (Fig. 4a). Nos. of FCM in left lateral lobe, right middle lobe and left middle lobe were 12.33 ± 3.27 , 8.83 ± 1.72 and 6.33 ± 2.34 , respectively (Table 1).

PCI of Hepatic Embolization

FCM could be clearly identified inside the occluded vessel in dehydrated livers (Figs. 4c and 5a). In Fig. 5b, an about 100- μm portal vein and its branches are clearly shown to be embolized by a 100- μm FCM. In Figs. 5c and d, FCM can be clearly distinguished from the wall of the vessel on axial view. The spatial distribution of FCM inside target vessels could be clearly revealed by 3D reconstruction application (Figs. 5e and f). The FCM could also be clearly revealed to identify the embolized segment of the non-dehydrated liver (Fig. 6).

Discussion

In order to prevent postoperative liver insufficiency, PVE is often clinically used to stimulate growth of the non-embolized liver segment [19–21]. The effect will be better if the embolic agents

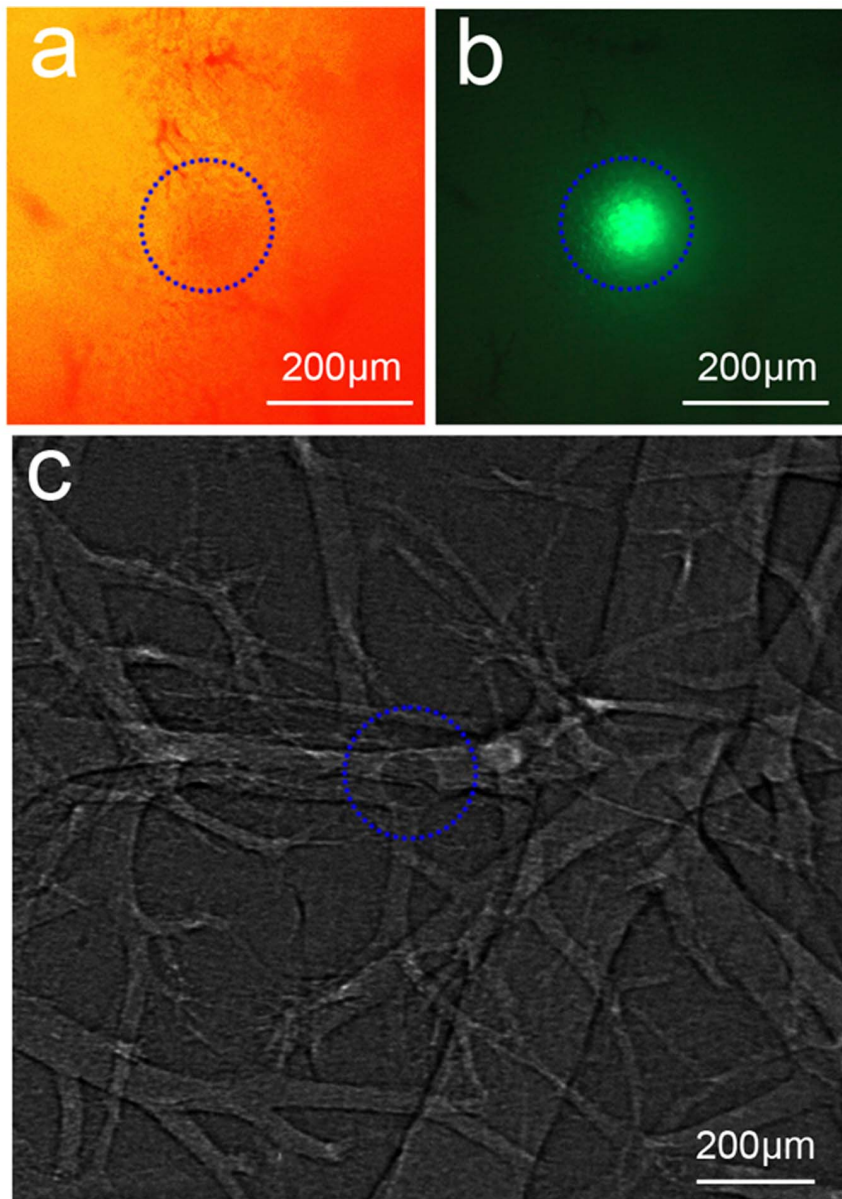


Figure 4. Microscopic observation and PCI of FCM-embolized liver. The fluorescent micrograph (b) shows FCM in the liver more clearly than optical micrograph (a). (c) A FCM can be clearly shown in the portal vein. The blue circles indicate FCM. Image was obtained at the energy of 19 keV with the sample-to-detector distance of 60 cm. The pixel size was $3.7 \mu\text{m} \times 3.7 \mu\text{m}$; the exposure time was 1 s.
doi:10.1371/journal.pone.0080919.g004

selectively block the blood supply that feeds the tumor. Accordingly, good knowledge of embolic spatial distribution is vital to

make embolization at the desired liver segment. The present study has for the first time reported that PCI has great potential for pre-clinical PVE investigation with radiolucent embolic agents.

Though the effects of x-ray scatters on the absorption contrast images are significantly reduced by using narrow SR x-ray beam, no distinct contrast between GS or PVA and its surrounding air could be observed by ACI. By increasing the sample-to-detector distance, in-line phase contrast can be obtained for the sample [22,23]. PCI has been shown to be quite suitable for liver research, such as liver fibrosis [24] and liver cancer [25]. PCI, unlike ACI, depends mainly on phase shift properties to offer greatly improved contrast for low-absorption materials [10,26,27]. The phase contrast technique can convert such phase shifts into intensity differences that can be detected directly. The two embolic agents present irregular in shape. However, the irregular shape and

Table 1. Nos. of FCM in three main lobes of liver.

Lobe of liver	No. of FCM	
	Mean	Standard deviation
Left lateral lobe	12.33	3.27
Right middle lobe	8.83	1.72
Left middle lobe	6.33	2.34

doi:10.1371/journal.pone.0080919.t001

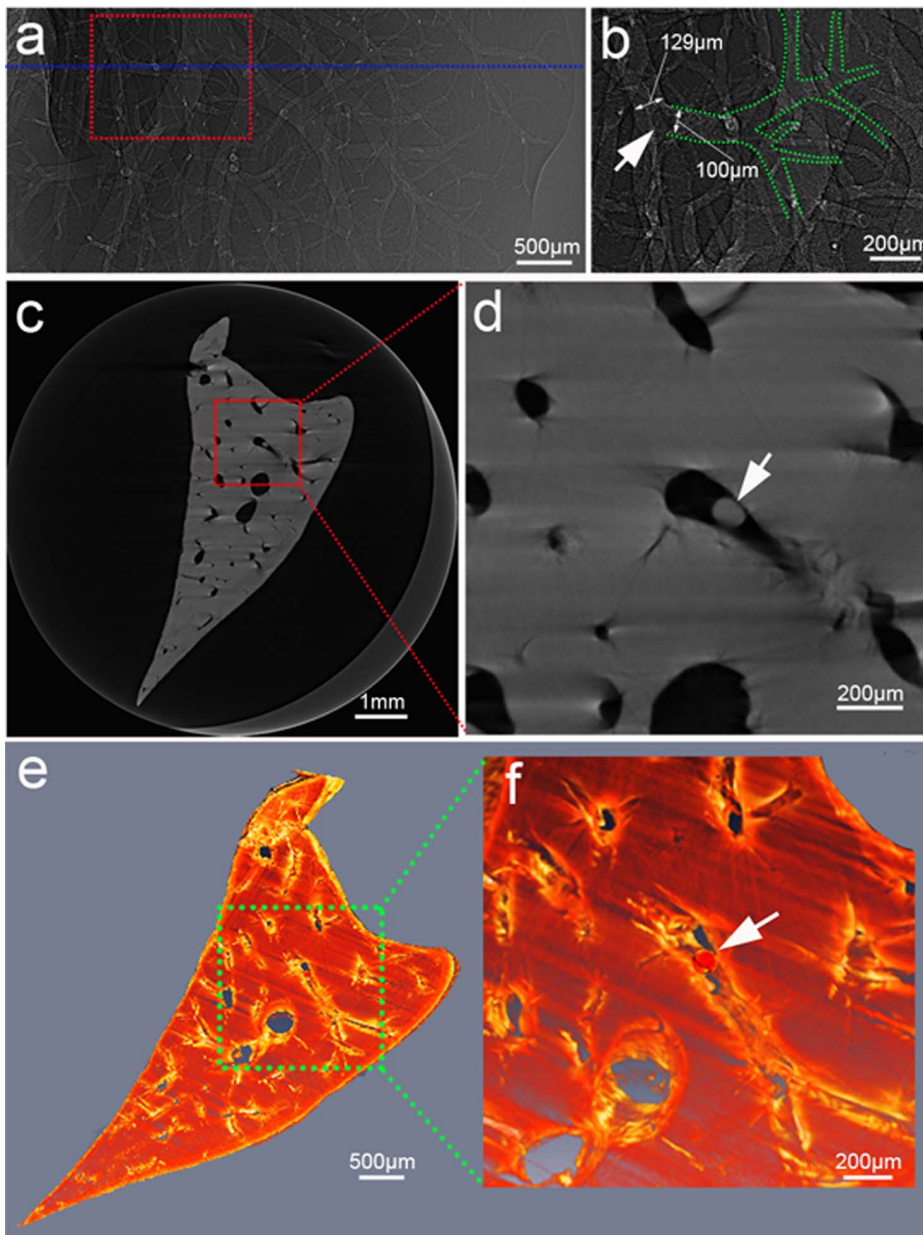


Figure 5. Phase contrast CT imaging of FCM-embolized dehydrated liver. Projection image (a) and reconstructed views (c,e) visibly show the FCM in the embolized portal vein. (b), (d) and (f) are magnified images of the region in a dotted box in (a), (c) and (e), respectively. (b) An about 100- μm portal vein and its branches (outlined in green) are clearly displayed to be embolized by a 100- μm FCM. (c) is the axial slice across the blue line in (a). (f) The 3D rendering shows spatial distribution of the microspheres inside the liver. Arrows indicate FCM. Images were obtained at the energy of 19 keV with the sample-to-detector distance of 60 cm. The pixel size was $3.7 \mu\text{m} \times 3.7 \mu\text{m}$; the exposure time was 1 s. doi:10.1371/journal.pone.0080919.g005

variable size of these particles may present a poor correlation of the occlusion level and the particle size [28]. When large particles are properly oriented, they can reach a distal vessel. In addition, the aggregation behavior of the particles may cause blockage of proximal large vessels rather than other desired vessels. Nowadays, spherical embolic agents with uniform shape have been developed to overcome the disadvantages of conventional embolic agents [28–30]. The microspheres can make a predictable occlusion of vessels according to the particle size selected. Here, we use spherical FCM as radiolucent embolic agents. The fluorescent characteristic of the microspheres can offer the potential for multimodal imaging. Because the difference between the absorp-

tion coefficients of FCM and air is small, no evident contrast can be detected by ACI. In comparison, PCI exploits the differences in the refractive index and enables clear visualization of the FCM.

The hepatic vessels were filled with air to replace blood after they were fully dehydrated. On PCI, the phase shifts arising from FCM-air interfaces can generate sufficient image contrast to show the weak-absorption FCM. After the injection, FCM run through vessels, and then stop when they reach vessel of their own size. Thus, the embolization level was directly related to the diameter of injected embolic agents. Many embolic beads were found in three main lobes of liver; still, some FCM retained in main portal vein. In further study, super-selective catheterization technique may be

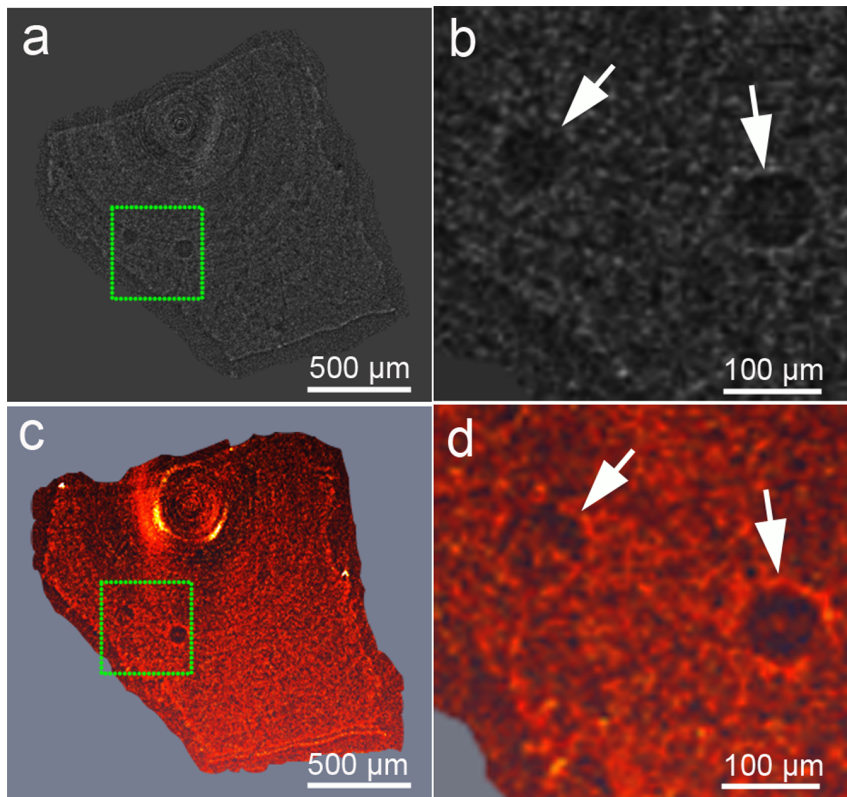


Figure 6. Phase contrast CT imaging of FCM-embolized non-dehydrated liver. Axial (a) and 3D (c) views of FCM in the liver. (b) and (d) are magnified images of the region in a dotted box in (a) and (c), respectively. Note that the phase contrast CT imaging clearly showed the radiolucent FCM in the liver tissues. Arrows indicate FCM. Images were obtained at the energy of 19 keV with the sample-to-detector distance of 60 cm. The pixel size was $3.7 \mu\text{m} \times 3.7 \mu\text{m}$; the exposure time was 1 s.
doi:10.1371/journal.pone.0080919.g006

used to concentrate the embolic agents in the targeted hepatic lobe. The phase contrast CT imaging could also provide adequate image contrast to distinguish the FCM from the non-dehydrated liver tissues; consequently, the embolized liver segment could be directly and obviously identified. Besides phase contrast, high spatial-resolution performance is another important characteristic for PCI using SR [31,32]. The spatial resolution of PCI can arrive at submicron scale, which is much higher than that of conventional angiography using x-ray, CT, and MRI [33–35]. On PCI, we could visualize vessels of about one-tenth of the diameter measured by conventional angiography. So PCI has the potential for imaging fine embolized vessels.

In summary, the characteristics of sensitivity to low-absorption materials and high resolution for PCI are very attractive. Compared with ACI, PCI is capable of creating remarkable visibility of radiolucent embolic agents. In addition, phase contrast

CT technology can help to noticeably reveal the 3D spatial distribution of low-absorption embolic agents and clearly identify the embolized liver segment. Therefore, PCI can be currently used for pre-clinical evaluation of new embolic agents in animal models; meanwhile, the imaging modality may allow potential medical application if a compact SR x-ray source is employed in the future.

Acknowledgments

The authors thank Yudan Wang, Yanan Fu and Heyu Chen for their kindly assistance in our experiments.

Author Contributions

Conceived and designed the experiments: RT. Performed the experiments: RT WH. Analyzed the data: RT FY WMC. Contributed reagents/materials/analysis tools: GYY YL KMC. Wrote the paper: RT.

References

1. Broering DC, Hillert C, Krupski G, Fischer L, Mueller L, et al. (2002) Portal vein embolization vs. portal vein ligation for induction of hypertrophy of the future liver remnant. *Journal of Gastrointestinal Surgery* 6: 905–913.
2. Furrer K, Tian Y, Pfammatter T, Jochum W, El Badry AM, et al. (2007) Selective portal vein embolization and ligation trigger different regenerative responses in the rat liver. *Hepatology* 47: 1615–1623.
3. Hartog A, Mills G (2009) Anaesthesia for hepatic resection surgery. *Continuing Education in Anaesthesia, Critical Care & Pain* 9: 1–5.
4. Madoff DC, Hicks ME, Vauthey JN, Charnsangavej C, Morello FA, et al. (2002) Transhepatic Portal Vein Embolization: Anatomy, Indications, and Technical Considerations. *Radiographics* 22: 1063–1076.
5. Madoff DC, Denys A, Wallace MJ, Murthy R, Gupta S, et al. (2005) Splenic Arterial Interventions: Anatomy, Indications, Technical Considerations, and Potential Complications. *Radiographics* 25: S191–S211.
6. Yoon W (2004) Embolic agents used for bronchial artery embolisation in massive haemoptysis. *Expert Opinion on Pharmacotherapy* 5: 361–367.
7. Zhang L, Hu C, Zhao T, Luo S (2011) Noninvasive visualization of microvessels using diffraction enhanced imaging. *European journal of radiology* 80: 158–162.
8. Bravin A, Coan P, Suortti P (2013) X-ray phase-contrast imaging: from pre-clinical applications towards clinics. *Physics in Medicine and Biology* 58: R1.
9. Tang R, Chai W-M, Ying W, Yang G-Y, Xie H, et al. (2012) Anti-VEGFR2-conjugated PLGA microspheres as an x-ray phase contrast agent for assessing the VEGFR2 expression. *Physics in Medicine and Biology* 57: 3051.

10. Tang R, Xi Y, Chai W-M, Wang Y, Guan Y, et al. (2011) Microbubble-based synchrotron radiation phase contrast imaging: basic study and angiography applications. *Physics in Medicine and Biology* 56: 3503.
11. Lewis R (2004) Medical phase contrast x-ray imaging: current status and future prospects. *Physics in Medicine and Biology* 49: 3573.
12. Tang R, Li W-X, Huang W, Yan F, Chai W-M, et al. (2013) CO₂-based in-line phase contrast imaging of small intestine in mice. *Scientific Reports* 3.
13. Arfelli F, Rigon L, Menk R (2010) Microbubbles as x-ray scattering contrast agents using analyzer-based imaging. *Physics in Medicine and Biology* 55: 1643.
14. Gao X, Luo S, Yin H, Liu B, Xu M, et al. (2006) A micro-tomography method based on X-ray diffraction enhanced imaging for the visualization of micro-organs and soft tissues. *Computerized Medical Imaging and Graphics* 30: 339–347.
15. Parsons DW, Morgan K, Donnelley M, Fouras A, Crosbie J, et al. (2008) High-resolution visualization of airspace structures in intact mice via synchrotron phase-contrast X-ray imaging (PCXI). *Journal of Anatomy* 213: 217–227.
16. Laperle CM, Hamilton TJ, Wintermeyer P, Walker EJ, Shi D, et al. (2008) Low density contrast agents for x-ray phase contrast imaging: the use of ambient air for x-ray angiography of excised murine liver tissue. *Physics in Medicine and Biology* 53: 6911.
17. Zhang X, Liu X-S, Yang X-R, Chen S-L, Zhu P-P, et al. (2008) Mouse blood vessel imaging by in-line x-ray phase-contrast imaging. *Physics in Medicine and Biology* 53: 5735.
18. Chen R-C, Dreossi D, Mancini L, Menk R, Rigon L, et al. (2012) PITRE: software for phase-sensitive X-ray image processing and tomography reconstruction. *Journal of Synchrotron Radiation* 19: 0–0.
19. Abdalla E, Hicks M, Vauthey J (2002) Portal vein embolization: rationale, technique and future prospects. *British Journal of Surgery* 88: 165–175.
20. Azoulay D, Castaing D, Smail A, Adam R, Cailliez V, et al. (2000) Resection of nonresectable liver metastases from colorectal cancer after percutaneous portal vein embolization. *Annals of Surgery* 231: 480.
21. Huang JY, Yang WZ, Li JJ, Jiang N, Zheng QB (2006) Portal vein embolization induces compensatory hypertrophy of remnant liver. *World Journal of Gastroenterology* 12: 408.
22. Snigirev A, Snigireva I, Kohn V, Kuznetsov S, Schelokov I (1995) On the possibilities of x-ray phase contrast microimaging by coherent high-energy synchrotron radiation. *Review of Scientific Instruments* 66: 5486–5492.
23. Wilkins S, Gureyev T, Gao D, Pogany A, Stevenson A (1996) Phase-contrast imaging using polychromatic hard X-rays. *Nature* 384: 335–338.
24. Zhang X, Yang X-R, Chen Y, Li H-Q, Li R-M, et al. (2013) Visualising liver fibrosis by phase-contrast X-ray imaging in common bile duct ligated mice. *European Radiology* 23: 417–423.
25. Tao Q, Li D, Zhang L, Luo S (2012) Using X-Ray In-Line Phase-Contrast Imaging for the Investigation of Nude Mouse Hepatic Tumors. *PLoS One* 7: e39936.
26. Simpson SJ, Siu KK, Yagi N, Whitley JC, Lewis RA, et al. (2013) Phase Contrast Imaging Reveals Low Lung Volumes and Surface Areas in the Developing Marsupial. *PLoS One* 8: e53805.
27. Hwang J, Kim M, Kim S, Lee J (2013) Quantifying Morphological Parameters of the Terminal Branching Units in a Mouse Lung by Phase Contrast Synchrotron Radiation Computed Tomography. *PLoS One* 8: e63552.
28. Osuga K, Maeda N, Higashihara H, Hori S, Nakazawa T, et al. (2012) Current status of embolic agents for liver tumor embolization. *International Journal of Clinical Oncology* 17: 306–315.
29. Laurent A, Wassef M, Saint Maurice J-P, Namur J, Pelage J-P, et al. (2006) Arterial distribution of calibrated tris-acryl gelatin and polyvinyl alcohol microspheres in a sheep kidney model. *Investigative Radiology* 41: 8–14.
30. Pelage J-P, Le Dref O, Beregi J-P, Nonent M, Robert Y, et al. (2003) Limited uterine artery embolization with trisacryl gelatin microspheres for uterine fibroids. *Journal of Vascular and Interventional Radiology* 14: 15–20.
31. Tang R, Chai W-M, Yang G-Y, Xie H, Chen K-M (2012) X-ray Phase Contrast Imaging of Cell Isolation with Super-Paramagnetic Microbeads. *PLoS One* 7: e45597.
32. Xi Y, Tang R, Wang Y, Zhao J (2011) Microbubbles as contrast agent for in-line x-ray phase-contrast imaging. *Applied Physics Letters* 99: 011101-011103.
33. Fink C, Kiessling F, Bock M, Lichy MP, Misselwitz B, et al. (2003) High-resolution three-dimensional MR angiography of rodent tumors: Morphologic characterization of intratumoral vasculature. *Journal of Magnetic Resonance Imaging* 18: 59–65.
34. Kitchen M, Lewis R, Yagi N, Uesugi K, Paganin D, et al. (2005) Phase contrast X-ray imaging of mice and rabbit lungs: a comparative study. *British Journal of Radiology* 78: 1018–1027.
35. Kobayashi S, Hori M, Dono K, Nagano H, Umeshita K, et al. (2004) In vivo real-time microangiography of the liver in mice using synchrotron radiation. *Journal of Hepatology* 40: 405–408.